Smart Tumor Homing for Manhattan-Like Capillary Network Regulated Tumor Microenvironment

Yin Qing[1], Yue Sun[1,2(✉)], Yue Xiao[1], and Yifan Chen[2]

[1] Chengdu University of Technology, Chengdu 610059, China
[2] University of Electronic Science and Technology of China, Chengdu 611731, China

Abstract. This paper investigates the tumor microenvironment regulated by the dense interconnected capillary network nearby, forming Manhattan-like biological gradient fields (BGFs) distribution. The research to date has tended to focus on modeling in Euclidean space rather than Manhattan space. Based on the Manhattan-like BGFs, we propose a coordinate gradient descent (CGD) iterative algorithm to realize tumor homing. Nanorobots with contrast agents and sensors are employed as computing agents. The sensors serve as local sensing agents to provide iterative information, and the contrast agents can deposit themselves on the tumor through the enhanced permeability and retention (EPR) to make magnetic resonance imaging (MRI) easier to detect. We aim to achieve tumor homing using as few iterations as possible in a Manhattan-like BGF. The simulation results show that the proposed CGD algorithm has higher efficiency and fewer iterations in Manhattan-like BGFs than the brute-fore.

Keywords: Tumor homing · Manhattan-like BGFs · CGD iterative algorithm

1 Introduction

Magnetic Nanoparticle-mediated drug delivery has drawn much attention in cancer theranostics. Since the presence of magnetic nanoparticles (MNPs) introduces inhomogeneities in the local magnetic field that increase the signal decay rate, resulting in a significant contrast change in the tissue enriched with MNPs [1]. Thus, magnetic resonance imaging (MRI) employs MNPs as contrast agents to enhance tumor detection [2]. The main problem facing this approach is the targeted delivery relies on systemic blood circulation and only less than 2% of the nanoparticles can deliver to a precise site [3]. Another alternative approach is an iterative-optimization-inspired direct targeting strategy (DTS) for nanosystems [4]. Nanoswimmers assembled by many magnetic nanoparticles are served as computing agents. In the presence of an external magnetic field, the

T. Nakano (Ed.): BICT 2021, LNICST 403, pp. 134–144, 2021.
https://doi.org/10.1007/978-3-030-92163-7_11

nanoswimmers are guided to potential sites of tumors. When the tumor binds to the contrast agents, the enhanced permeability and retention (EPR) effect will be triggered, thus enabling tumors to be detected by MRI [5]. One of the other methods is a self-regulated and coordinated targeting strategy, inspired by the collaborative movements of the living cells in different natural biological processes [6]. This method doesn't require an external centralized control unit, nanoparticle swarm cooperates and coordinates autonomously through the information provided by the biological gradient fields (BGFs), and carries out tumor homing in the search domain.

The growth of tumors affects the microenvironment around, changing its physical properties. For instance, 60% of solid cancers contain hypoxic areas heterogeneously dispersed throughout the tumor [7]. Some tumors rely on glycolysis to produce energy, which leads to hypoxic concentration and acidosis, increasing the spatial distribution differences in tumor areas [8]. The biophysical information, regulated by capillary networks, is presented as a multi-dimensional BGFs distribution. The two alternative methods mentioned above both use BGFs as objective functions to provide iterative direction information and consider it as a continuous distribution in a Euclidean space.

This paper introduces BGFs similar to taxicab geometry. To deliver the oxygen to the tissues efficiently, capillaries shape as an even-distributed, two-dimensional grid network, as shown in Fig. 2(a) [9]. The formation of BGFs is related to the capillary network. The oxygen content levels in the blood decrease as the distance from the arterial end increases [10]. Therefore, tumor cells located at the distal end of the blood vessel may be hypoxic, even if they are close to the vessel [11]. Due to the lack of oxygen, cells produce lactic acid anaerobic respiration, resulting in a decrease in PH [12]. The formation of these BGFs has been inseparable from the capillary network, which is a Manhattan space. Therefore, so when considering an actual BGF, a Manhattan space should more suitable than Euclidean space.

Recent work improves the detection probability and targeting efficiency employing external magnetic field control of nanorobots [4]. The major advantage of tumor sensitization through external manipulation is that the route to reach the lesion tissues is optimal and minimization the risk of exposure to the systemic circulation. A similar and holistic approach is employed, integrating nanorobots with sensors, an external centralized control unit, and Manhattan-like BGFs for a tumor homing. We modify objective functions into Manhattan-like objective functions, the coordinate gradient descent (CGD) is the iterative search algorithm in a Manhattan space. For the acquisition of the iterative direction, using sensors to local sensing in vivo, an external controlling and tracking system, such as an integrated device consisting of pairs of electromagnetic coils to generate a rotating magnetic field [13] to drive the nanorobots.

The paper is organized as follows. In Sect. 2, potential errors of BGFs being an objective function are discussed, and the transformation from Euclidean metric objective functions to Manhattan-like objective functions are presented. Section 3 demonstrates the CGD algorithm and the acquisition of discrete

gradient. Next, numerical simulations are performed to validate the effectiveness of the proposed algorithm in Sect. 4. Finally, Sect. 5 consists of the conclusion of this paper and future works.

2 Manhattan-Like Objective Function

BGFs can be divided into two types, environment-response and environment-primed. The first type can be obtained by using the physical properties of the tumor microenvironment, such as low pH, alteration in oxygen content, and blood velocity [10]. Special nanoparticles are injected into the blood flow to create an artificial BGF accumulated in the vicinity of the tumor. For instance, modified gold nanorods can accumulate in tumors through systemic circulation passively [14].

Tumor-induced BGFs can be used as auxiliary information for in vivo computing and provide evaluation criteria for position information of nanorobots. To understand and measure BGFs computationally, the objective functions with global maximum are considered to represent the possible situation of BGFs of in vivo computation. Assume that $\mathbb{D}$ denotes the high-risk area of the tumor. Then computing agents are represented by G. The objective functions based on Manhattan- and Euclidean-space are represented by F and f, respectively. As computational agents of in vivo computing, nanorobots are composed of natural materials that will physically, chemically, and biologically react with living tissues, which indicates that the interactions between agent G and the domain $\mathbb{D}$ induces disturbance, resulting in measurement error. Therefore, the objective function can be described as follows:

$$\mathrm{F}(\boldsymbol{x};\mathrm{G}) = F_T(\boldsymbol{x}) + \epsilon(\boldsymbol{x};G) \qquad \boldsymbol{x} \in \mathbb{D} \tag{1}$$

where $F_T(\boldsymbol{x})$ is the true objective function value at $\boldsymbol{x}$. $\epsilon(\boldsymbol{x};G)$ is the random compensation error, which attempts to counteract the disturbance caused by G.

As mentioned above, BGFs in the capillary shape like a grid model, which further refers to a Manhattan space. Currently, the functions used in many standard testing problems are mostly Euclidean metrics. However, the test function in the Euclidean metric is continuous and derivable everywhere, unlike the Manhattan metric, which is defined only orthogonally. Thus, the Euclidean metric is not suitable for describing the proposed Manhattan-like BGFs. Therefore, we modify a Euclidean metric-based objective function into Manhattan-based. In order for our modifications to have more practical implications, the transformation derives from the physical definition differences between the Manhattan and Euclidean metric, which indicates that area and distance formed by BGFs are different in Manhattan space and Euclidean space.

Give two points (x_n, y_n), (x_m, y_m) and a expression as:

$$(x_m - x_n) * (y_m - y_n) \tag{2}$$

at the Euclidean metric-based (2) can represent the rectangular area with side lengths $\sqrt{(x_m - x_n)^2}$ and $\sqrt{(y_m - y_n)^2}$. Recalculated using Manhattan metric-based definition, the side length can be expressed as $|x_m - x_n|$ and $|y_m - y_n|$. Therefore, the area of rectangle can be modified as:

$$|x_m - x_n| * |y_m - y_n| \tag{3}$$

Similarly, the mapping table between Euclidean metric-based and Manhattan metric-based is given in Table 1 as a reference for modifying a Manhattan-like function.

Table 1. Mapping table from euclidean metric-based to manhattan metric-based.

Euclidean metric-based function	Manhattan-like function
$\sqrt{x^2 + y^2}$	$\|x\| + \|y\|$
x	$\|x\|$
$x - y$	$\|x\| - \|y\|$
$x * y$	$\|x\| * \|y\|$
x^3	$\|x\|^3$
x^2	$\|x\|^2$

Different objective functions are employed to describe the BGFs of the tumor in related works. In this paper, these objective functions in Euclidean space are modified to Manhattan-like functions, with the maximum and minimum value being normalized to 1 and 0, respectively. Then the selected search field is limited to a square with a side length of 10 mm.

1) Bowl-shaped

$$f(x, y) = 1 - 0.14\left(\sqrt{x^2 + y^2}\right) \qquad (\mathrm{x}, \mathrm{y}) \in \mathbb{V} \tag{4}$$

The modifying result is as follows:

$$F(x, y) = 1 - 0.14(|x| + |y|) \qquad (\mathrm{x}, \mathrm{y}) \in \mathbb{V} \tag{5}$$

2) Plate-shaped

$$f(x, y) = 1 - \left(0.01\left(x^2 + y^2\right) + 0.02xy\right) \quad (\mathrm{x}, \mathrm{y}) \in \mathbb{V} \tag{6}$$

The modifying result is as follows:

$$F(x, y) = 1 - \left(0.01\left(|x|^2 + |y|^2\right) + 0.02|x||y|\right) \quad (\mathrm{x}, \mathrm{y}) \in \mathbb{V} \tag{7}$$

where $\mathbb{V}$ represents the capillary grid network. As shown in Fig. 1, the modified Manhattan-like functions are taken as the objective functions where the maximum value represents the location of the tumor. The numebr 0.14 reported in both (4) and (5), and the numbers 0.01 and 0.02 reported in (6) and (7) are the normalization coefficients, they do not affect the performance of the algorithm when the objective functions are used as test functions. The contour plots of the modified Manhattan-like functions are diamond-shaped, which is consistent with the situation in a Manhattan space. The gradient of the Bowl-shaped function is smooth and uniform, considered as the best case of BGFs. And the gradient of the Plate-shaped function is not as smooth as Bowl-shaped, therefore it can be treated as a general case of BGFs.

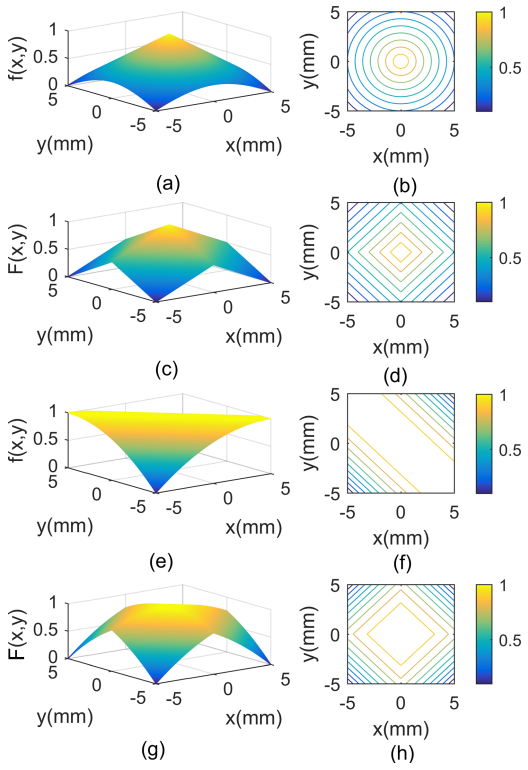

Fig. 1. Graphical representation of two objective functions. (a) Bowl-shaped and (b) its contour plot; (c) Bowl-shaped modified to manhattan-like results and (d) its contour plot; (e) Plate-shaped and (f) its contour plot; (g) Plate-shaped modified to manhattan-like results and (h) its contour plot. All objective functions have a maximum value of 1 and a minimum value of 0.

The capillary network consists of straight and rigid cylindrical blood vessels [15], and fractal models are often used to describe their bifurcation structure. However, fractal models cannot imitate the interconnected structure of the capillary network, especially in the vicinity of the tumor, which can be more appropriately described with a grid model [9]. In our model, the capillary is regarded as a grid model with an equal side length Δd. Then, the Manhattan-like objective function is mapped to the grid model. As shown in Fig. 2(b), only four vertices of each grid are used as the mapping results. The blue circles, represent possible path points after mapping, the red trajectory represents the iterative path of the agents.

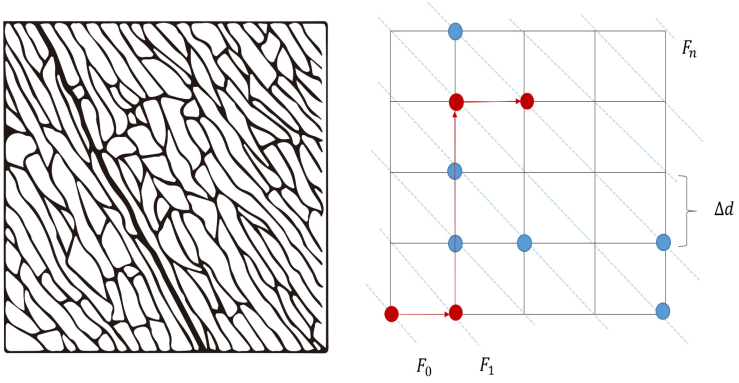

Fig. 2. (a) Blood vessels in microvasculature [9]; (b) Capillary network grid model and points on the grid that intersects $F_0 - F_n$ represent the equipotential points.

3 Coordinate Gradient Descent

The previous section has shown that the grid model of the capillary network is a Manhattan space. Therefore, it is necessary to adopt a Manhattan detection trajectory, which means subject the detect direction of the agents to limitations. Assuming that the blood flow direction is from lower left to upper right, then the actual detect direction of agents becomes upward or right. Thus, we propose the CGD iterative algorithm based on the gradient descent algorithm [4] and coordinate descent [16], which limits the direction of the gradient to the direction of the coordinate axis in order to conform to the detection of a Manhattan space.

Firstly, the discrete derivatives can be described as:

$$F'(x) = \frac{F(x + \Delta d) - F(x)}{\Delta d} \tag{8}$$

where Δd is the grid width as shown in Fig. 2(b). $F(x + \Delta d)$ is the value of objective function at location $x + \Delta d$, measured by the agents. The iteration position of agents is updated as follows:

$$\boldsymbol{x}_{k+1} = \boldsymbol{x}_k + \Delta\boldsymbol{x} + s_{k+1}\boldsymbol{u}_{\angle\varphi+\Delta\varphi} \tag{9}$$

where $\Delta\boldsymbol{x}$ is the location error, $\boldsymbol{u}_{\angle\varphi}$ is a unit vector with a direction angle φ. In CGD the specific value of φ is 0 or $\frac{\pi}{2}$. $\Delta\varphi$ is the angular deviation, due to the steering magnetic field and agents steering imperfections. We simply assume that $\Delta\boldsymbol{x}$, $\Delta\varphi$ are all subject to the variance of $\sigma^2_{\Delta x}$, $\sigma^2_{\Delta\varphi}$ and the mean of 0 normal distribution. s_{k+1} is the step size of the k+1-th iteration, the AdaGrad is employed to calculate the step size for each iteration. The step size updates as follows:

1) Accumulated derivative square

$$r_k = r_{k-1} + \left(F'_k\right)^2 \tag{10}$$

2) Update step size

$$s_k = s_{k-1} - F'_k\left(\frac{s_{k-1}}{\delta + \sqrt{r_k}}\right) \tag{11}$$

where $r_0 = 0$, F'_k is the discrete derivative can be obtained from (8). In the calculation process, to avoid the value of r_k being 0, a constant $\delta = 10^{-7}$ is added to the denominator to ensure the stability of the numerical value, which will not affect the update of step size. The update in the y-axis direction is the same as that in the x-axis. The pseudocode of the CGD iterative algorithm is as shown in Algorithm 1.

Algorithm 1. Coordinate gradient descent (CGD)

Input: Objective function $F(x, y)$, initialize agent location: $\boldsymbol{x}_0$, $\boldsymbol{y}_0$, initial step size : s, constant $\delta = 10^{-7}$, initialize discrete derivative accumulation variables: r_x, r_y

Output: Maximum value of objective function: F_{min}

while Stop criteria not reached **do**
  Fix the x-axis direction, treat variable x as constant;
  repeat
    Calculate the discrete derivative in y direction d_y;
    Accumulate discrete derivatives, update r_y;
    Calculate and update step size:s_y;
    Calculate the next position of the agent in the y direction;
    Update agent location;
  until Find that local optimal solution in the y-axis direction
  Fix the y-axis direction, treat variable y as constant;
  Repeat the process of finding the local optimal solution on the y-axis;
end while

Finally, compared with the traditional mathematical optimization process, the CGD has constraints of in vivo computing. The initial location of the agents

is limited to a small area, which is the injection point, instead of the whole detection domain. If agents outside the detection domain, new agents will be injected at the initial point to ensure the balance of the total agents.

4 Simulation Results

To validate our model and verify the performance of the proposed CGD algorithm, numerical simulations are complemented through MATLAB. The search range is $(-5\,\text{mm},5\,\text{mm})$, vessel spacing is 0.1 mm, tumor radius is 0.5 mm, and the maximum number of iterations is set to 200. Two Manhattan-like functions modified in Sect. 2 are used as objective functions, and the initial position of agents is limited to $-5\text{ mm} \leq \text{x},\text{y} \leq -4\text{ mm}$. Two indicators, the iterations K and the effective rate ξ, are introduced to evaluate the efficiency of the CGD algorithm. ξ is the ratio of the number of agents successfully staying in the tumor area to the number of general agents injected. In the simulation, three agents are injected at the same time, We assume that each agent is independent in the computation process. For comparison, brute-force search is also performed in the objective functions, in which the agents wander upward and right randomly at each point.

The initial injection locations of the agents are set as $(-5,-5)$, $(-4,-5)$, $(-4.5,-4.5)$. Any agent staying in the tumor area is recognized to have successfully detected for the tumor. As shown in Fig. 3, the red trajectories represent the CGD algorithm and the black trajectories represent the brute-force.

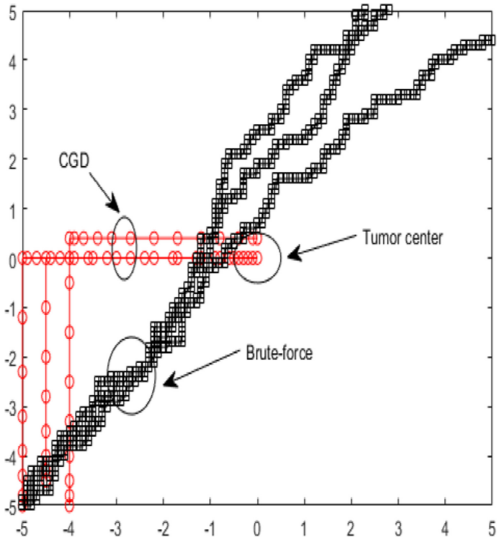

Fig. 3. The red cycles represent the trajectories of the CGD, while the black cubes represent the trajectories of the "brute-force". Agents stay in the tumor area are regarded as a successful homing. (Color figure online)

In the simulation results, because of its randomness, brute-force failed to detect tumor most of the time and the iteration number k of successful detection was approximately 100. And the simulation results of the CGD iterative algorithm are presented in the Table 2. In terms of the simulation results, CGD can detect the tumor location with a higher ξ and fewer K for both different objective functions.

Table 2. K and ξ of the CGD

Objective functions(F)	Initial positions	Iterations(K)	The effective rate(ξ)
Bowl-shaped	(−5,−5)	22	50%
	(−4,−5)	20	
	(−4.5,−4.5)	22	
Plate-shaped	(−5,−5)	26	83%
	(−4,−5)	25	
	(−4.5,−4.5)	26	

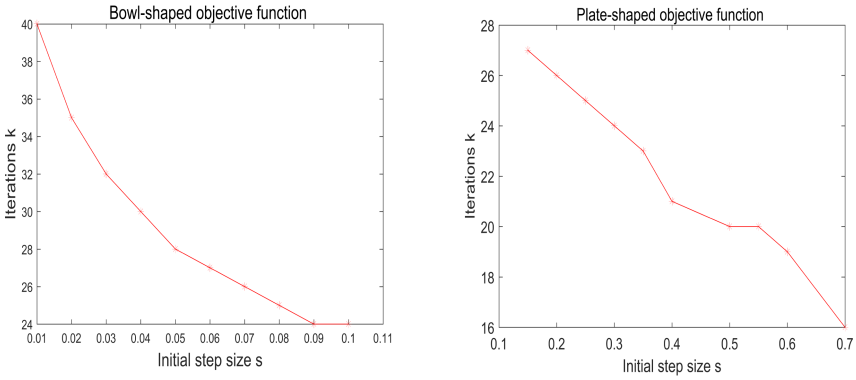

(a) (b)

Fig. 4. (a) For Bowl-shaped objective function, the influence of initial step size on the number of iterations(K); (b) For Plate-shaped objective function, the influence of initial step size on the number of iterations(K).

Due to the limitation of blood flow direction, nanorobots simply move from one side to the other, quite differ from traditional numerical optimization where computing agents can freely reciprocate in search space. Therefore, the setting of optimal parameters should be different in optimization algorithms for in vivo computing. In our simulation experiments, the selection of the initial step size

has a prominent effect on K. As shown in Fig. 4, an increase in initial step size will diminish the number of K. If the initial step size is extremely small, the agents do not have exploration ability at the beginning of the calculation. And if the initial step size exceeds a certain range would result in the poor discovery of the intended tumor location. This indicates that the initial step size is the main parameter of the searching process.

5 Conclusion

This paper introduces Manhattan-like BGFs and exhibits the transformation of objective functions in different dimensions. In addition, we propose a CGD iterative algorithm in a Manhattan-like space to homing tumor and validate its performance through the simulation. This work has enhanced our understanding of BGFs distribution. Further work should focus on more factors of Manhattan-like BGFs formed by tumors. Finally, the tumor homing process should involve external centralized control to ensure the iterations of the agents.

References

1. Friedrich, R.M., et al.: Magnetic particle mapping using magnetoelectric sensors as an imaging modality. Sci. Rep. **9**(1), 1–11 (2019)
2. Thoidingjam, S., Tiku, A.B.: New developments in breast cancer therapy: role of iron oxide nanoparticles. Adv. Nat. Sci. Nanosci. Nanotechnol. **8**(2), 023002 (2017)
3. Bae, Y.H., Park, K.: Targeted drug delivery to tumors: myths, reality and possibility. J. Controlled Release **153**(3), 198 (2011)
4. Chen, Y., Ali, M., Shi, S., Cheang, U.K.: Biosensing-by-learning direct targeting strategy for enhanced tumor sensitization. IEEE Trans. NanoBiosci. **18**(3), 498–509 (2019). https://doi.org/10.1109/TNB.2019.2919132
5. Kasban, H.: A comparative study of medical imaging techniques. Int. J. Inf. Sci. Intell. Syst., **4**, 37–58 (2015)
6. Ali, M., Sharifi, N., McGrath, N., Cree, M.J., Chen, Y.: Self-regulated and coordinated smart tumor homing for complex vascular networks. In: 2020 42nd Annual International Conference of the IEEE Engineering in Medicine Biology Society (EMBC), pp. 378–381 (2020). https://doi.org/10.1109/EMBC44109.2020.9176014
7. A, P.V.: Tumor microenvironmental physiology and its implications for radiation oncology. Seminars in Radiation Oncology **14**(3), 198–206 (2004)
8. Helmlinger, G., Yuan, F., Dellian, M., Jain, R.K.: Interstitial ph and po2 gradients in solid tumors in vivo: high-resolution measurements reveal a lack of correlation. Nat. Med. **3**(2), 177–182 (1997)
9. Baish, J.W., Gazit, Y., Berk, D.A., Nozue, M., Jain, R.K.: Role of tumor vascular architecture in nutrient and drug delivery: an invasion percolation-based network model. Microvasc. Res. **51**(3), 327–346 (1996)
10. Gray, M., Meehan, J., Turnbull, A.K., Martínez-Pérez, C., Argyle, D.J.: The importance of the tumor microenvironment and hypoxia in delivering a precision medicine approach to veterinary oncology. Front. Vet. Sci. **7**, 907 (2020)

11. Dewhirst, M.W., Ong, E.T., Braun, R.D., Smith, B., Klitzman, B., Evans, S.M., Wilson, D.: Quantification of longitudinal tissue po2 gradients in window chamber tumours: impact on tumour hypoxia. Br. J. Cancer **79**(11), 1717–1722 (1999)
12. Srensen, B.S., Horsman, M.R.: Tumor hypoxia: Impact on radiation therapy and molecular pathways. Front. Oncol. **10**, 562 (2020)
13. Cheang, U.K., Meshkati, F., Kim, H., Lee, K., Fu, H.C., Min, J.K.: Versatile microrobotics using simple modular subunits. Sci. Rep. **6**, 30472 (2016)
14. Agemy, L., Sugahara, K.N., Kotamraju, V.R., Gujraty, K., Ruoslahti, E.: Nanoparticle-induced vascular blockade in human prostate cancer. Blood **116**(15), 2847–2856 (2010)
15. Mcdougall, S.R., Anderson, A., Chaplain, M., Sherratt, J.A.: Mathematical modelling of flow through vascular networks: Implications for tumour-induced angiogenesis and chemotherapy strategies. Bull. Math. Biol. **64**(4), 673–702 (2002)
16. Onose, A., Dumitrescu, B.: Adaptive randomized coordinate descent for solving sparse systems. In: Adaptive Randomized Coordinate Descent for Solving Sparse Systems, IEEE (2014)